High resolution planar encoder by retro-reflection

Ching-Fen Kao, Sheng-Hua Lu, and Mao-Hong Lu

Articles you may be interested in

Development of a three-degree-of-freedom laser linear encoder for error measurement of a high precision stage
Rev. Sci. Instrum. **78**, 066103 (2007); 10.1063/1.2743165

Use of two-photon polymerization for continuous gray-level encoding of diffractive optical elements
Appl. Phys. Lett. **90**, 073503 (2007); 10.1063/1.2426923

Two-dimensional tracking of a motile micro-organism allowing high-resolution observation with various imaging techniques
Rev. Sci. Instrum. **76**, 034301 (2005); 10.1063/1.1857632

High resolution optical shaft encoder for motor speed control based on an optical disk pick-up
Rev. Sci. Instrum. **69**, 3068 (1998); 10.1063/1.1149057

Measurement of position and orientation of optical elements in interferometric gravity wave detectors
Rev. Sci. Instrum. **68**, 3197 (1997); 10.1063/1.1148267

High resolution planar encoder by retro-reflection

Ching-Fen Kao[a)]
*Department of Photonics & Institute of Electro-Optical Engineering, National Chiao Tung University,
Hsinchu, Taiwan 30050, Republic of China*

Sheng-Hua Lu
Department of Photonics, Feng Chia University, Taichung, Taiwan 300, Republic of China

Mao-Hong Lu
*Department of Photonics & Institute of Electro-Optical Engineering, National Chiao Tung University,
Hsinchu, Taiwan 30050, Republic of China*

This investigation presents a planar diffractive laser encoder system (PDLENS), which serves as a two-dimensional (2D) position detection apparatus for precision machine applications. Traditional 2D position detection utilizes a pair of linear encoders in crossed construction and so maintaining the perpendicularity between this pair of encoders is difficult. Besides, the rigorous alignment requirements among various components of the encoder system impose a serious user adaptation bottleneck. Of all alignment tolerances, the head-to-scale alignment tolerance is the most important problem for applications. In this work, a 2D grating is employed as the scale and the PDLENS is based on the retro-reflection configuration. Therefore the new encoder can provide good perpendicularity and tolerate larger alignment errors than the conventional encoder does. The grating pitch is 1.6 μm and the period of the output signal is 0.4 μm due to the double diffraction. Electronic interpolation with a factor of 400 leads to a readout resolution of 1 nm. The new encoder and a capacitive sensor were employed to simultaneously measure a circular motion with a radius of 1 μm generated by a piezo stage. Comparing the measured positions, the deviation is less than 30 nm and the repeatability is better than 8 nm. © *2005 American Institute of Physics.*
[DOI: 10.1063/1.2006368]

I. INTRODUCTION

As nanometer resolution technology has rapidly advanced, biological systems, materials, and manipulative systems have entered the nanometer regime. All of these applications require planar substrate stages for sample scanning. These stages with nanometer resolution generally employ heterodyne laser displacement measuring interferometers (DMI) or capacitive displacement sensors (Cap sensor) to locate the moving positions of stages. But Cap sensors have a limit to a long traveling range. DMI sensors provide a high resolution and a long traveling range in sensing displacement. However, the DMI sensors have the disadvantage of being bulky and expensive, and are difficult to integrate into compact systems.[1] The accuracy of high-performance planar stages depends on the alignment of the workpiece platform with the interferometer's mirrors.

A laser encoder system is developed for two-dimensional, long-distance, nano-scale positioning and so it is suitable for semiconductor or scanning probe microscopy measurement applications. Many of today's state-of-the-art laser planar encoder designs apply either geometrical[2] or diffractive[3,4] principles of optics. Other designs using the waveguide technique[5] or fluorescent dye method can also be found in the literature.

The planar encoder includes an optical head and a diffractive grating. The main problem in broadening the applications of the planar encoders is that the optical head must be aligned with micrometer precision relative to the diffractive grating and be held to tight tolerances during system operation. The need for production machines to operate at high speed is very important for current industries such as semiconductors, hard disks, and liquid crystal display manufacturing. Faster operating speeds of the machines typically correspond to larger mechanical wobble or vibration. The wobble or vibration between the optical head and the operating machine, where the grating scale is mounted, directly influence the quality of the optical signals and so make the optoelectronic signals decay or even disappear. Restated, false or null measurements are made when wobble occurs.

Our previous work[6] reported a planer encoder, which is based on the diffraction principle. The design, which uses one grating scale and pairs of retro-reflective optics, has the advantage of improving the tolerance of head-to-scale mechanical wobble. The retro-reflection of these encoders provides an interference scheme with equal optical path. Consequently, the highly visible or contrasting interference fringes can be seen. However, the last design applies a beam splitter to produce two incident beams for two-dimensional (2D) displacement. The light intensity is almost lost on grating diffraction. This work presents a new optical design, in which a corn cube is used as a retro-reflective optical device. 2D

[a)]Also affiliated with Center for Measurement Standards, Hsinchu, Taiwan 300, R.O.C.; electronic mail: alicekao@itri.org.tw
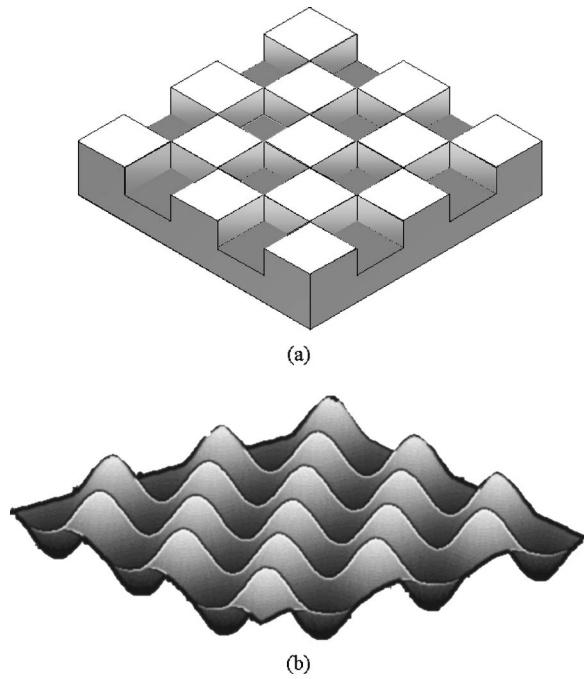
(a)

(b)

FIG. 1. 2D gratings. (a) The 2D grating with rectangular profile (rectangular grating). (b) The 2D grating with sinusoidal profile (sinusoidal grating).

displacement can be obtained by only one grating and one incident beam. So, the new design improves the efficiency of light and simplifies the fabrication.

II. THEORY

A. Diffraction by 2D grating

A laser beam was normally incident on a 2D grating with equivalent periods in both directions. The grating was located in the X-Y plane. The direction of the light diffracted by the 2D grating with equivalent periods in both directions can be written as[7,8]

$$\sin\theta = \frac{\sqrt{\nu_x^2 + \nu_y^2}}{\sqrt{\nu_x^2 + \nu_y^2 + \nu_z^2}} = \frac{\sqrt{\left(\frac{m}{p}\right)^2 + \left(\frac{n}{p}\right)^2}}{\left(\frac{1}{\lambda}\right)} = \frac{\sqrt{m^2 + n^2}\lambda}{p}. \quad (1)$$

Here p is the period of the grating, ν_x is m/p, and ν_y is n/p. The Ewald sphere is given by $\nu_x^2 + \nu_y^2 + \nu_z^2 = (1/\lambda)^2$, λ is the wavelength. θ is the angle between the diffractive ray and the normal to the grating. The 2D grating equation, Eq. (1), determines the direction of the (m,n) diffraction order. The surface relief depth and spatial frequency of the 2D grating directly influence the diffraction efficiency and the output polarization states of the diffracted waves.[8,9] The software GSOLVER based on the rigorous coupled wave theory is used to design the profile of a 2D grating for an incident beam with circle polarization. Two types of profile are considered. Figure 1(a) shows the 2D grating with a rectangular profile (rectangular grating), and Fig. 1(b) displays the 2D grating with a sinusoidal profile (sinusoidal grating). Figure 2 represents the relationship between the diffraction efficiency for the relief depth of the grating. In Fig. 2(a), the four orders of diffraction $(\pm1,\pm1)$ from the 2D rectangular grating have maximum efficiency for a surface relief depth of 250 nm. In Fig. 2(b), the four orders of diffraction $(\pm1,0),(0,\pm1)$ of the
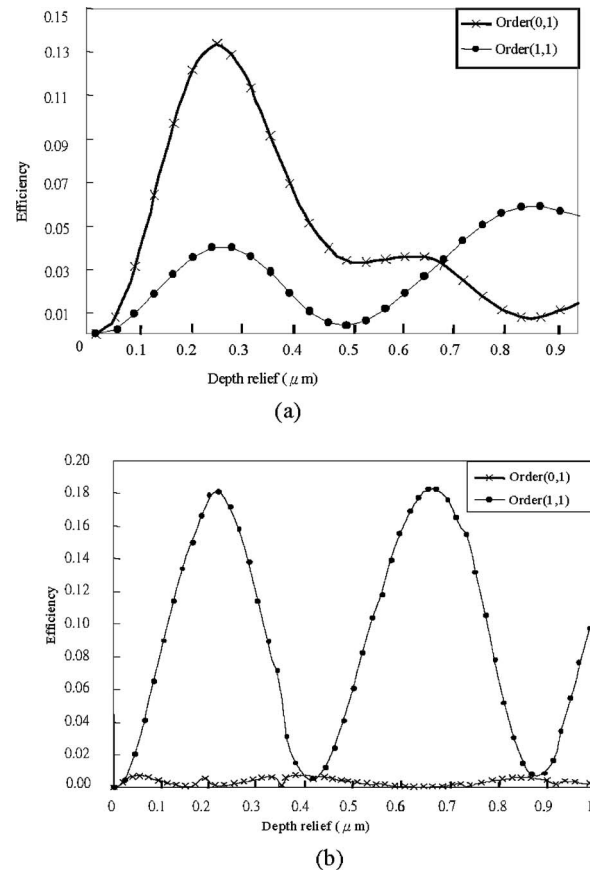

(a)

(b)

FIG. 2. The relation between the diffraction efficiency and the grating depth. (a) The efficiency of 2D rectangular grating. (b) The efficiency of 2D sinusoidal grating.

2D sinusoidal grating have maximum efficiency, and a surface relief depth of 210 nm. These results demonstrate that both types of gratings can be used for planar encoders.

B. Configurations and operational principles

According to Sec. II A, the four first-diffraction orders $(\pm1,0),(0,\pm1)$ of the 2D sinusoidal grating are regarded as a first-type planar encoder. As shown in Fig. 3(a), a laser beam is normally incident on a 2D sinusoidal grating with equivalent periods in both directions. The grating is located in the X-Y plane. The incident plane-wave is $U_{in} = A_0 \exp(-ikz)$, where A_0 is the amplitude of the incident light, and $k = 2\pi/\lambda$ is the wave number. The wave vector of the incident light can be written as $k_{in} = -k\hat{z}$, where $\hat{z}$ is the unit vector in the z direction. According to Eq. (1), the four first-diffraction orders $(m=\pm1, n=0)$, and $(m=0, n=\pm1)$ are on the X-Z and Y-Z planes, respectively, of the Cartesian coordinate system. The first-diffraction field is denoted by $U_{s1}(m,n)$. As displayed in Fig. 3(b), the four beams of first diffraction are retro-reflected by corner cubes and returned to the 2D sinusoidal grating to generate double diffraction. The double-diffraction order is denoted by $(m,n;m',n')$, where (m',n') represents the order of the double diffraction and (m,n) represents the order of the original diffraction which produces the double diffraction. The double-diffraction field is denoted by $U_{s2}(m,n;m',n')$. The first-diffraction field $U_{s1}(1,0)$ of

the 2D sinusoidal grating, and double-diffraction field $U_{s2}(1,0;1,0)$ can be expressed as

$$U_{s1}(1,0) = A_1\exp\left(ik_{1,0}z + i2\pi\frac{x}{p}\right)$$

$$= A_1\exp(ikz\cos\theta)\exp(ikx\sin\theta),$$

$$U_{s2}(1,0;1,0) = A_2\exp\left(-ik_{1,0;1,0}z - i2\pi\frac{x}{p}\right)\exp\left(i2\pi\frac{x}{p}\right)$$

$$= A_2\exp(ikz), \tag{2}$$

where A_1 is the amplitude of the first diffraction, A_2 is the amplitude of the double diffraction, and $\sin\theta = \lambda/p$.

The change of angular frequency is considered to elucidate the interference phenomenon with the Doppler effect[10,11] as the displacement occurs between the 2D grating and incident light. In Fig. 3(b), $\boldsymbol{k}_{s1}$ represents the wave vector of the first order of diffraction $U_{s1}(1,0)$, and $\boldsymbol{k}_{s2}$ represents the wave vector of the double-diffraction order $U_{s2}(1,0;1,0)$. According to Eq. (2), the wave vector of light can be expressed as

$$\boldsymbol{k}_{in} = -k\hat{z},$$

$$\boldsymbol{k}_{s1} = k\sin\theta\,\hat{x} + k\cos\theta\,\hat{z}, \tag{3}$$

$$\boldsymbol{k}_{s2} = k\hat{z}.$$

The change of the angular frequency is given by

$$\Delta\omega_{s1} = (\boldsymbol{k}_{s1} - \boldsymbol{k}_{in})\cdot\boldsymbol{V}_g + [\boldsymbol{k}_{s2} - (-\boldsymbol{k}_{s1})]\cdot\boldsymbol{V}_g,$$

$$= 2\cdot(\boldsymbol{k}_{s1} + \boldsymbol{k}_{s2})\cdot\boldsymbol{V}_g, \tag{4}$$

where $\boldsymbol{V}_g$ is the velocity of the 2D grating and is written as $\boldsymbol{V}_g = V_{gx}\hat{x} + V_{gy}\hat{y}$. The change of the angular frequency can be determined by substituting Eq. (3) into Eq. (4). The result is

$$\Delta\omega_{s1} = 2(k\sin\theta\,\hat{x} + k\cos\theta\,\hat{z} + k\hat{z})\cdot(V_{gx}\hat{x} + V_{gy}\hat{y})$$

$$= 2k\sin\theta\cdot V_{gx}. \tag{5}$$

Similarly, in Fig. 3(b) the wave vector of the first-diffraction field $U_{s1}(-1,0)$ is represented by $\boldsymbol{k}'_{s1}$; the wave vector of the double-diffraction field $U_{s2}(-1,0;-1,0)$ by $\boldsymbol{k}'_{s2}$, and the wave vector of the incident light by $\boldsymbol{k}_{in}$. The wave vector of light can be expressed as

$$\boldsymbol{k}_{in} = -k\hat{z},$$

$$\boldsymbol{k}'_{s1} = -k\sin\theta\,\hat{x} + k\cos\theta\,\hat{z}, \tag{6}$$

$$\boldsymbol{k}'_{s2} = k\hat{z}. \tag{7}$$

The change of the angular frequency can be described as

$$\Delta\omega_{s2} = -2k\sin\theta\cdot V_{gx}. \tag{8}$$

The double-diffraction fields $U_{s2}(1,0;1,0)$ and $U_{s2}(-1,0;-1,0)$ propagate in the same direction ($\boldsymbol{k}_{s2} = \boldsymbol{k}'_{s2} = k\hat{z}$). Therefore, the amplitude distributions can be expressed as
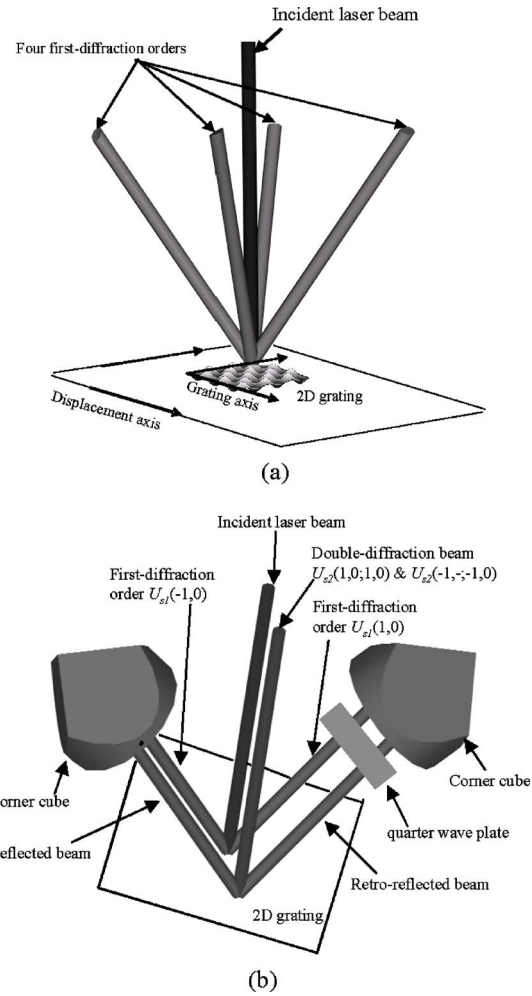

(a)

(b)

FIG. 3. (a) The incident light is diffracted into four first-diffraction orders. (b) The four first-diffraction orders are retro-reflected by corner cube.

$$E_1 = A_2 e^{i[(\omega + \Delta\omega_1)t + \phi_0]}, \tag{9}$$

$$E_2 = A_2 e^{i[(\omega + \Delta\omega_2)t + \phi_0]}. \tag{10}$$

The light intensity I_x of the superposition of the two beams is given by

$$I_x \propto |E_1 + E_2|^2 = |A_2|^2[2 + 2\cos(\Delta\omega_2 - \Delta\omega_1)t] = |A_2|^2[2$$

$$+ 2\cos(4k\sin\theta\cdot\Delta x)] = |A_2|^2\left[2 + 2\cos\left(\frac{8\pi\Delta x}{p}\right)\right],$$

$$\tag{11a}$$

where Δx is the displacement in the X direction. Likewise, the light intensity due to the displacement in Y direction can be expressed as

$$I_y = |A_2|^2\left[2 + 2\cos\left(\frac{8\pi\Delta y}{p}\right)\right], \tag{11b}$$

where Δy is the grating displacement in the Y direction. The two-dimensional displacement can be obtained as stated earlier.

In the second-type planar encoder, the 2D rectangular grating is considered. The four first-diffraction beams, $(\pm 1, \pm 1)$, of the 2D rectangular grating have maximum efficiency, and the four first-diffraction beams ($m = \pm 1, n = \pm 1$)
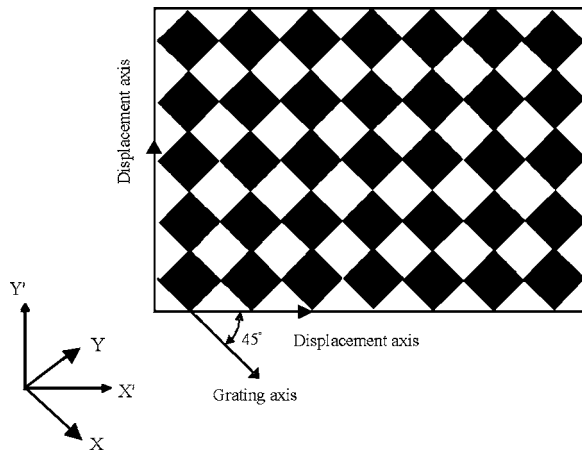
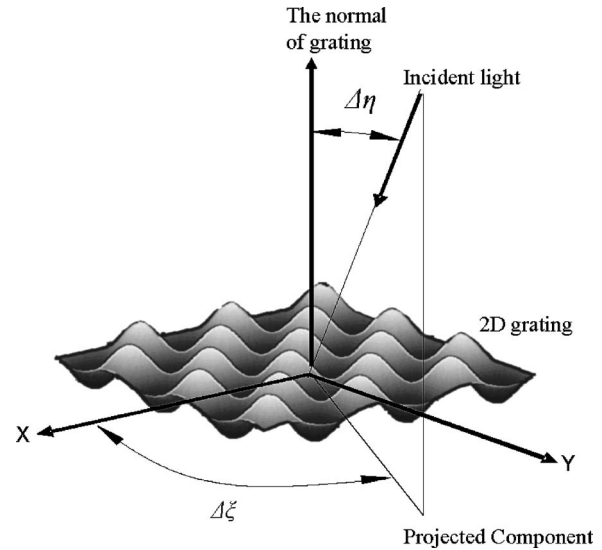FIG. 4. The 2D rectangular grating makes an angle of 45° with the axes of the movement.

FIG. 5. Tilt between incident beam and 2D grating. The angle between the incident light and the normal to the grating is $\Delta\eta$. The azimuth angle is $\Delta\xi$.

are in the four quadrants of the Cartesian coordinate system. As mentioned earlier, the first-diffraction field of 2D rectangular grating $U_{t1}(1,1)$, and the double-diffraction field $U_{t2}(1,1;1,1)$ can be expressed as

$$U_{t1}(1,1) = A_1\exp\left[ik_{1,1}z + i2\pi\frac{(x+y)}{p}\right]$$
$$= A_1\exp(ikz\cos\theta)\exp\left[i\frac{(x+y)}{\sqrt{2}}k\sin\theta\right],$$

$$ \tag{12} $$

$$U_{t2}(1,1;1,1) = A_2\exp\left(-ik_{1,1;1,1}z - i\frac{2\pi(x+y)}{p}\right)$$
$$\cdot\exp\left(i\frac{2\pi(x+y)}{p}\right) = A_2\exp(ikz),$$

where A_1 is the amplitude of first diffraction, and A_2 is the amplitude of double diffraction. The wave vector of the first-diffraction field $U_{t1}(1,1)$ is denoted by k_{t1}, and the double-diffraction field $U_{t2}(1,1;1,1)$ is k_{t2}. According to Eq. (2), the wave vector of light can be expressed as

$$k_{in} = -k\hat{z},$$

$$k_{t1} = \frac{k}{\sqrt{2}}\sin\theta\,\hat{x} + \frac{k}{\sqrt{2}}\sin\theta\,\hat{y} + k\cos\theta\,\hat{z}, \tag{13}$$

$$k_{t2} = k\hat{z}.$$

Similarly, the wave vector of the first-diffraction field $U_{t1}(-1,-1)$ is k'_{t1}, the wave vector of the double-diffraction field $U_{t2}(-1,-1;-1,-1)$ is k'_{t2}, and that of the incident light is k_{in}. The wave vector of light can be expressed as

$$k_{in} = -k\hat{z},$$

$$k'_{t1} = -\frac{k}{\sqrt{2}}\sin\theta\,\hat{x} - \frac{k}{\sqrt{2}}\sin\theta\,\hat{y} + k\cos\theta\,\hat{z}, \tag{14}$$

$$k'_{t2} = k\hat{z}.$$

Figure 4 demonstrates that the axes on which the grating lies make an angle of 45° with the axes of movement. A counterclockwise rotation by 45° around the z axis trans-

forms the coordinate system (x,y) to the system (x',y'). The wave vector of light k_{t1} and k'_{t1} can be rewritten as

$$k_{t1} = k\sin\theta\,\hat{x}' + k\cos\theta\,\hat{z},$$

$$ \tag{15} $$

$$k'_{t1} = -k\sin\theta\,\hat{x}' + k\cos\theta\,\hat{z}.$$

The change of the angular frequency with the motion of the grating can be described as follows;

$$\Delta\omega_{t1} = 2k\sin\theta\cdot V_{gx'},$$

$$\Delta\omega_{t2} = -2k\sin\theta\cdot V_{gx'}.$$

The two-dimensional displacement can be obtained as mentioned earlier. The light intensities I_x and I_y of interference are given by

$$I_{x'} \propto \left[2 + 2\cos\left(\frac{8\pi\Delta x'}{p}\right)\right], \tag{16a}$$

$$I_{y'} \propto \left[2 + 2\cos\left(\frac{8\pi\Delta y'}{p}\right)\right], \tag{16b}$$

where $\Delta x'$ is the displacement in the $\hat{x}'$ direction and $\Delta y'$ is the displacement in $\hat{y}'$ direction. Based on the above discussions, both gratings can be used as grating scales for two-dimensional displacement encoders (planar encoders).

C. Alignment tolerance analysis

Two kinds of errors influence the signal quality of a planar encoder. One is from the mechanical wobble between the optical head and the grating scale. The other is from the installation errors when the system is manufactured. The latter can be corrected by precise alignments, however, the mechanical wobble cannot be avoided during machine operation. This system provides a large head-to-scale alignment tolerance.

Figure 5 reveals that the mechanical wobbles between the optical head and the grating scale cause an angle change of the incident light upon the grating scale. The angle change

is described by angle $\Delta\eta$ between the incident light and the normal of the grating scale, and the azimuthal angle $\Delta\xi$. The wave vectors of the incident light and diffraction beams in Eq. (3) thus become

$$\boldsymbol{k}_{\mathrm{in}} = -k(\sin\Delta\eta\cos\Delta\xi)\hat{x} - k(\sin\Delta\eta\sin\Delta\xi)\hat{y}$$
$$- k(\cos\Delta\eta)\hat{z},$$

$$\boldsymbol{k}_1 = k(-\sin\Delta\eta\cos\Delta\xi + \sin\theta)\hat{x}$$
$$+ k(-\sin\Delta\eta\sin\Delta\xi)\hat{y} + k_{1Z}\hat{z}, \qquad (17)$$

$$\boldsymbol{k}_2 = (k\sin\Delta\eta\cos\Delta\xi)\hat{x} + (k\sin\Delta\eta\sin\Delta\xi)\hat{y}$$
$$+ (k\cos\Delta\eta)\hat{z}.$$

The change of the angular frequency caused by the Doppler effect can be rewritten as

$$\Delta\omega_1 = (\boldsymbol{k}_1 - \boldsymbol{k}_{\mathrm{in}})\cdot\boldsymbol{V}_g + [\boldsymbol{k}_2 - (-\boldsymbol{k}_1)]\cdot\boldsymbol{V}_g = 2(k\sin\theta\,\hat{x}$$
$$+ k\cos\theta\,\hat{z})\cdot(V_{gx}\hat{x} + V_{gy}\hat{y}) = 2k\sin\theta\cdot V_{gx}. \quad (18)$$

Similarly, Eq. (6) becomes

$$\boldsymbol{k}_{\mathrm{in}} = -k(\sin\Delta\eta\cos\Delta\xi)\hat{x} - k(\sin\Delta\eta\sin\Delta\xi)\hat{y}$$
$$- k(\cos\Delta\eta)\hat{z},$$

$$\boldsymbol{k}'_1 = k(-\sin\Delta\eta\cos\Delta\xi - \sin\theta)\hat{x}$$
$$+ k(-\sin\Delta\eta\sin\Delta\xi)\hat{y} + k_{1Z}\hat{z}, \qquad (19)$$

$$\boldsymbol{k}'_2 = (k\sin\Delta\eta\cos\Delta\xi)\hat{x} + (k\sin\Delta\eta\sin\Delta\xi)\hat{y}$$
$$+ (k\cos\Delta\eta)\hat{z}.$$

The change of the angular frequency is

$$\Delta\omega_2 = -2k\sin\theta\cdot V_{gx}. \qquad (20)$$

Equations (17) and (19) imply that the two double-diffraction beams propagate in the same direction ($\boldsymbol{k}_2 = \boldsymbol{k}'_2$) though the wobble causes the encoder head to tile from the scale grating. Equations (18) and (20) mean that the tilt between the encoder head and the scale grating does not affect the changes of the angular frequency $\Delta\omega_1$ and $\Delta\omega_2$. Therefore, the angle between the optical head of the encoder and the grating was automatically compensated for without affecting the measurement of displacement in this configuration.

III. EXPERIMENT AND RESULTS

The retro-reflection of these encoders provides an interference scheme with equal path lengths. This equal path configuration can obtain a fringe contrast of near 100%. Therefore, a low coherence light source, such as a diode laser, can be used. The diode laser, guided by a fiber and collimated by a lens, is used as a light source. The collimated light is incident on a 2D grating and diffracted to produce four first-diffraction beams. The four beams of the first diffraction are retro-reflected by four corner cubes, which returned them to the 2D grating to produce double diffraction. Phase shift sig-
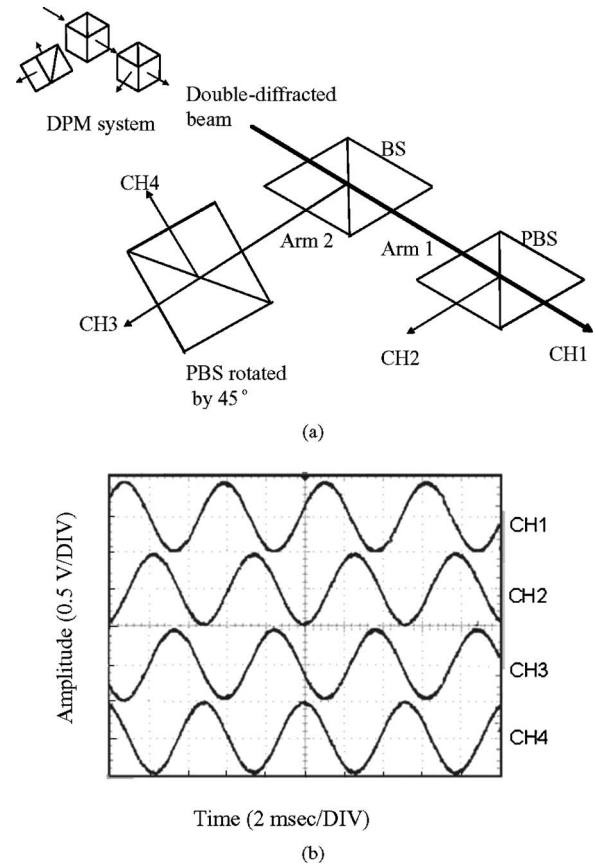

FIG. 6. (a) A scheme for phase shift module. The phase of the four arms can be shifted by increments of 90°. (b) The four orthogonal sinusoidal signals.

nals produce four orthogonal sinusoidal signals (sine and cosine) to determine the direction of movement, eliminate common-mode noise, and increase the resolution by interpolation. Smyth and Moore presented the phase shift method in their work of instantaneous phase shifting interferometry.[12–14] The phase shift technique is called direct phase measurement (DPM). As shown in Fig. 3(b), a quarter wave plate is inserted into one path of retro-reflected optics. The right-hand circularly polarized beam passes twice through the quarter wave plate and the polarization becomes left-handed. The polarizations of the two double-diffraction beams that propagate in the same direction become orthogonal. The combined beam (two double-diffraction beams) is directed to DPM. Figure 6 displays DPM with four channels. The combined collimated beam (two double-diffraction beams) is made to travel through the nonpolarizing beam splitter and so splits into two arms. A polarizing beam splitter is introduced into each arm, so the two beams splits into four polarized beams. A photodetector is placed in each channel to detect the interference. Figure 6(a) indicates that one polarizing beam splitter was rotated by 45° around the optical axis. Hence the polarization direction shifted the relative phase by 90° between channels 1 and 3, and by 180° between channels 1 and 2. The above discussion shows that phase among the four channels can shift by increments of 90°. Figure 6(b) plots the four orthogonal sinusoidal signals.

A piezo-positioning system with a scanning range of 20 μm and nanometer resolution is used to measure the ac-
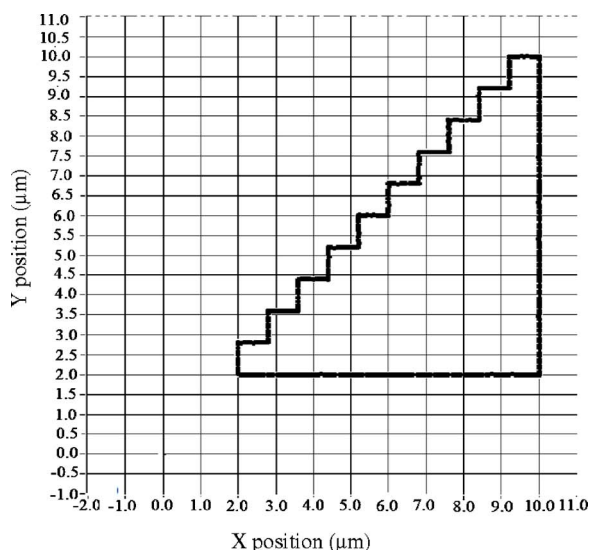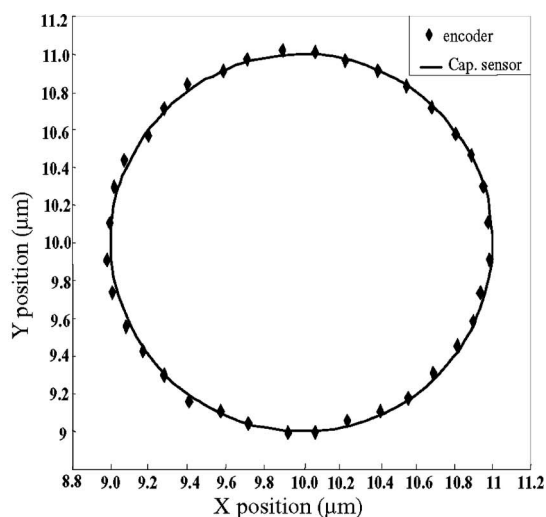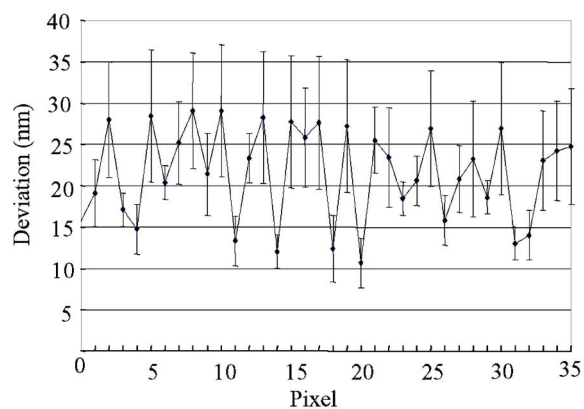
(a)
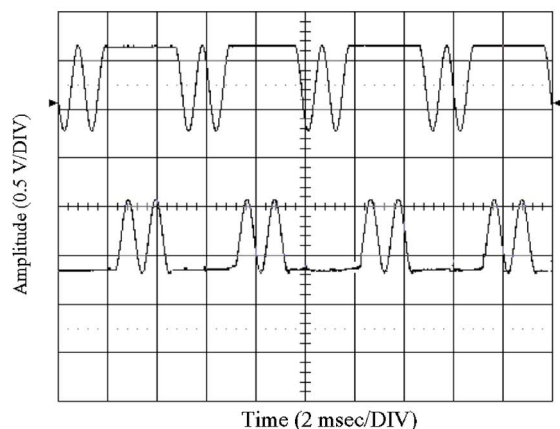
(b)

FIG. 7. (a) The stage moved in a step locus. (b) The generated sinusoidal signals when the stage moved in a step locus.

(a)

(b)

FIG. 8. (a) Circle motion measured by the capacitive displacement sensor and the planar encoder. (b) The differences between the measurements and the standard deviation of the repeatability measurements.

curacy of the planar encoder. The positioning system uses a flexure stage with a high mechanical stiffness and highly accurate guidance, a linearity of 0.1% and a repeatability of ±5 nm provided by an internal Cap sensor. Figure 7(b) shows the generated sinusoidal signals when the stage is moved in a step locus as shown in Fig. 7(a). The step locus signal shows that the planar encoder can separately record the X- and Y-axis displacements.

The output beams of the new encoder consist of two pairs of double-diffraction beams. The two double-diffraction beams of either pair are always collinear even though the scale grating is tilted by a wobble. This advantage arises from the retro-reflection configuration. However, the tilt of the grating changes the entrance positions of the first-diffraction beams. In this experiment, the beam diameter is 1 mm, the aperture of the corner cubes is 3.75 mm, the detector size is 3 mm, and the distance between the grating and conjugate optics is 15 mm. Therefore, the lateral shift of the first-diffraction beams must be less than $(3.75-1)/2 = 1.375$ mm to keep the beam always within the aperture of the corner cube. This requirement gives the head-to-scale tolerance to be $\Delta\eta = \sin^{-1}(1.375/15) = 5.25°$.

The period of the sinusoidal signals from the encoder head is 0.4 μm, which is one quarter of the scale pitch due to double diffraction. The signal period is subdivided by a counter board with an interpolation factor of 400 (HEIDEN-HAIN IK 220),[15] which leads to a readout resolution of 1 nm. The stage was programmed to move along a circle locus with a radius of 1 μm as shown in Fig. 8(a). Figure 8(b) is the deviation diagram along the circular path. The pixels are the sampling points, and the deviation is defined as $\sqrt{(x_e-x_c)^2+(y_e-y_c)^2}$, where (x_c,y_c) and (x_e,y_e) are the positions measured by the Cap sensor and planar encoder, respectively. This experiment was repeated ten times. The deviations are less than 30 nm and the standard deviations are around 8 nm, which results from the periodic error of 2D gratings, nonlinearity of the positioning system, and noises of electronic circuit.

[1] M. L. Schattenburg and H. I. Smith, *Proceedings of the SPIE Workshop on Nanostructure Science, Metrology and Technology*, 2001, Vol. 4608, pp. 1–8.

[2] S. Ichikawa, M. Suzuki, W. Ishibashi, and S. Kuroki, U.S. Patent 5,204,524, 1993.

[3] H. Huber and M. Aligauer, U.S. Patent 5,424,833, 1995.

[4] M. Hercher, U.S. Patent 5,530,543, 1996.

[5] H. Huber and M. Aligauer, U.S. Patent 5,493,397, 1996.

[6] C.-F. Kao, C. C. Chang, and M.-H. Lu, Opt. Eng. **44**, 023603 (2005).

[7] J. W. Goodman, *Introduction to Fourier Optics* (1968).

[8] H. J. Caulfield, *Handbook of Optical Holography* (1983), Chap. 2, pp. 40–43.

[9] M. G. Moharam and T. K. Gaylord, Proc. IEEE **73**, 894 (1985).

[10] *Handbook of Optics* (1996), Vol. 2, Chap. 30, p. 18.

[11] W. J. Wu, C. K. Lee, and C. T. Hsieh, Publication Office, Jpn. J. Appl. Phys., Part 1 **38**, 1725 (1999).

[12] R. Smyth and R. Moore, Opt. Eng. **23**, 361 (1984)

[13] N. R. Sivakumar, W. K. Hui, K. Venkatakrishnan, and B. K. A. Ngoi, Opt. Eng. **42**, 367 (2003).

[14] B. K. A. Ngoi, K. Venkatakrishnan, and N. R. Sivakumar, Opt. Commun. **190**, 109 (2001)

[15] IK 220 pc counter card user's manual, *Heisdehain Corporation*, March 2002.